International Journal of Applied Earth Observation and Geoinformation 130 (2024) 103887

Contents lists available at ScienceDirect

International Journal of Applied Earth Observation and Geoinformation

journal homepage: www.elsevier.com/locate/jag

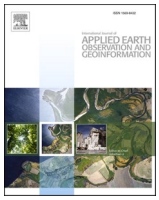

Examining the potential and effectiveness of water indices using multispectral sentinel-2 data to detect soil moisture as an indicator of mudflow occurrence in arid regions

Zahraa Al-Ali [a], Ammar Abulibdeh [b,*], Talal Al-Awadhi [c,d,**], Midhun Mohan [e,f], Noura Al Nasiri [c], Mohammed Al-Barwani [c], Sara Al Nabbi [c], Meshal Abdullah [a,c,g]

[a] Natural Environmental Systems and Technologies (NEST) Research Group, Ecolife Sciences Research and Consultation, Kuwait
[b] Applied Geography and GIS Program, Department of Humanities, College of Arts and Sciences, Qatar University, P.O. Box: 2713, Doha, Qatar
[c] Geography Department, College of Arts and Social Sciences, Sultan Qaboos University, Muscat, P.O. Box 42, P.C. 123, Oman
[d] Department of Geo-information Processing, Faculty of Geo-Information Science and Earth Observation, University of Twente, Enschede, Netherlands
[e] Department of Geography, University of California—Berkeley, Berkeley, CA 94709, USA
[f] Ecoresolve, San Francisco, CA 94105, USA
[g] Department of Ecology and Conservation Biology, Texas A&M University, College Station, TX 77843, USA

ARTICLE INFO

Keywords:
Spectral reflectance curve
Soil-line method
Spectral indices
Flood
Shaheen cyclone

ABSTRACT

This study aims to evaluate the performance and effectiveness of six spectral water indices - derived from Multispectral sentinel-2 data - to detect soil moisture and inundated area in arid regions to be used as an indicator of mudflow phenomena to predict high-risk areas. Herein, the validation of the performance of spectral indices was conducted using threshold method, spectral curve performance, and soil-line method. These indirect validation techniques play a key role in saving time, effort, and cost, particularly for large-scale and inaccessible areas. It was observed that the Normalized Difference Water Index (NDWI), Modified Normalized Difference Water Index (mNDWI), and RSWIR indices have the potential to detect soil moisture and inundated areas in arid regions. According to the temporal spectral curve performance, the spectral characteristics of water and soil moisture were distinct in the Near infrared (NIR) and Short-wave Infrared (SWIR1,2) bands. However, the rate and degree differed between these bands, depending on the amount of water in the soil. Furthermore, the soil line method supported the appropriate selection of threshold values to detect soil moisture. However, the threshold values varied with location, time, season, and between indices. We concluded that considering the factors influencing the behavior of water and soil reflectivity could support decision-makers in identifying high-risk mudflow locations.

1. Introduction

Mudflow is a common hazardous phenomenon that occurs during and after cyclones, causing a direct impact on agricultural areas and cities in terms of economic losses and compromised human well-being (Perera et al., 2018; Rao et al., 2019; FAO, 2021). Mudflow events have multiplied in the past years due to the significant increase in the frequency of cyclones and rainfall events as a result of climate change impacts (Mamadjanova and Leckebusch, 2022). The distribution of mudflow varies depending on the topography and soil type (Castro et al., 2020; Somos-Valenzuela et al., 2020). For instance, high-potential mudflow occurs in locations with steep slopes where the mud and debris rush downward due to gravitational force (Volgina and Sergeev, 2021). However, in low-slope topography, soil types - such as clay - are responsible for increasing the probability of mudflow occurrence (Vallejo, 1980). In other words, clay soil has a higher water-holding capacity and dries out less than other types of soil (Ismail and Ozawa, 2007), as clay soils have fine grains stacked together and tiny pores that make it highly moisturized in comparison with other soils (Morris and Energy, 2006). Thus, soil moisture can be considered an essential factor in an initial mudflow event (Marino et al., 2020). Variations in soil moisture can influence infiltration during rainfall storms (Peranić et al., 2022)

* Corresponding author.
** Corresponding author at: Geography Department, College of Arts and Social Sciences, Sultan Qaboos University, Muscat, P.O. Box 42, P.C. 123, Oman.
E-mail addresses: aabulibdeh@qu.edu.qa (A. Abulibdeh), alawadhi@squ.edu.om (T. Al-Awadhi).

https://doi.org/10.1016/j.jag.2024.103887
Received 21 March 2024; Received in revised form 23 April 2024; Accepted 30 April 2024
Available online 7 May 2024

and hence can indicate the probability of mudflow occurrence.

Measuring and analyzing soil moisture before and after an intense rainfall event can enhance our understanding of the probability of mudflow occurrence by helping to indicate high-risk areas. Methods including gravimetric, evaporation, leaching, and chemical reactions are considered direct traditional techniques used to determine the water content in the soil (Cooper, 2016). In-situ field instruments, such as electromagnetic sensors, gamma radiation sensors, neutron probes, and heat pulse probes, have also been used to measure soil moisture (Babaeian et al., 2019). However, these laboratory methods and instruments are only adequate for small areas to provide quantitatively accurate point-based field measurements; they are time-consuming and expensive for large-scale monitoring (Şekertekin et al., 2018).

The rapid development of remote sensing technologies has allowed the assessment and monitoring of spatio-temporal natural phenomena at small and large scales using optical, thermal, microwave, and radar data (Yue et al., 2019). Over the last decade, soil moisture has been widely studied worldwide, with a focus on different applications such as the prediction and monitoring of drought, hydrological processing, agricultural plant production, and landslide hazard assessment (Babaeian et al., 2019; Zhao et al., 2021). However, most of the studies used coarse spatial resolution, such as Soil Moisture and Ocean Salinity (SMOS) data (Gheybi et al., 2019), Soil Moisture Active and Passive (SMAP) data (Ma et al., 2017), Advanced Scatterometer (ASCAT) data (Brocca et al., 2017), and Advanced Microwave Scanning Radiometer (AMSR) data (Zhang et al., 2017). These coarse satellite data are adequate for monitoring soil moisture at a large scale, especially because they can revisit the same area every 1–5 days. Despite providing these satellites with high temporal resolution, the coarse resolution (25–50 km) could affect the output data at the local scale (Zhang et al., 2022). Some recent studies have utilized high-resolution images such as sentinel-1A to detect soil moisture (Zribi et al., 2019; Wang et al., 2022). Sentinel-1A is a satellite of the European Space Agency (ESA) based on Synthetic Aperture Radar (SAR), with high spatial (10 m) and temporal resolutions (12 revisit days) (https://sentinels.copernicus.eu/web/sentinel/missions/sentinel-1). However, the radar backscattering coefficient is sensitive to variations in soil conditions (roughness and soil types), topography, and vegetation cover (Parida et al., 2022).

Furthermore, certain studies have used medium-resolution multispectral data to detect soil moisture based on the relationship between vegetation indices and land surface temperature (LST) (Younis and Iqbal, 2015; Natsagdorj et al., 2019; Lu et al., 2020). Other studies have developed various water extraction algorithms using multispectral data, including spectral water indices, single-band thresholding, classification methods, and principal component analysis (PCA) (Acharya et al., 2018; Huang et al., 2018; Wen et al., 2021). For instance, Acharya et al. (2022) evaluated different spectral indices using Landsat-8 data to detect soil moisture in agricultural fields, including the Normalized Difference Vegetation Index (NDVI), Normalized Difference Water Index (NDWI), Normalized Difference Moisture Index (NDMI), Enhanced Vegetation Index (EVI), Structure-Insensitive Pigment Index (SIPI), and Atmospherically Resistant Vegetation Index (ARVI). They found a poor relationship between these indices and field soil moisture, which was highly affected by crop growth stages and vegetation cover. Serrano et al. (2019) found a significant correlation between soil moisture and NDWI derived from sentinel-2 imagery implemented in the Mediterranean agro-silvo-pastoral system. Reis et al. (2021) investigated a single threshold over the MNDWI to extract water bodies using Landsat-8 and sentinel-2 imageries. Sajjad et al. (2020) found that the mNDWI produced good results in delineating flood-inundated areas in Pakistan, with an overall accuracy of 90 % compared with NDWI (85 %) and Water Ratio Index (WRI) (82 %). Hence, hydrological monitoring studies have mainly focused on four aspects: detecting soil moisture using coarse satellite data, delineating surface water using water indices, implementing methods in agricultural areas, and validating the performance of remote sensing data using field data. Besides, limited studies investigate the dynamic changes in soil moisture in arid regions by quantifying the correlation between soil moisture and mudflow events using multispectral data (Gheybi et al., 2019).

The essential questions that need to be considered are: First, can water indices-based open-access multispectral data with high resolution provide satisfactory results for detecting soil moisture? Second, how can the performance of indices be validated when access to the areas is difficult or when investigating large-scale areas that would increase the cost of fieldwork? Thus, this study aims to investigate the potential and effectiveness of water indices using multispectral sentinel-2 data with a spatial resolution of 10 m and a temporal resolution of 5 days to detect soil moisture in arid regions. Six common water indices were evaluated in Oman as part of a Shaheen cyclone case study. Different indirect validation techniques were implemented to evaluate the performance of the examined indices, owing to the lack of field data.

The outcome of this study is expected to support decision-makers in identifying locations of high-risk mudflow areas for successful management, including land-use planning projects that delineate zoning regulations, infrastructure planning, and protecting agricultural areas. This will be done by considering soil moisture as an indicator of mudflow occurrence, especially in low-slop topography and clay soil.

2. Study area

This study was conducted in the Al-Batinah area in the northern part of the Sultanate of Oman, along the west shore of the Gulf of Oman, nearly 300 km Northwest of Muscat, the capital city of Oman, and at the edge of the Western Hajar Mountains in the northeastern part of the country (Fig. 1A, B). The study area is approximately 1738 km^2, situated between 56.841 °N and 24.034 °N. It was highly impacted by the Shaheen cyclone, which hit Oman on Oct 3, 2021 (Al-Awadhi et al., 2024). Its geographic location makes Oman be exposed to the most extreme climatic events. The climate of the region is classified as a Tropical and Subtropical Desert Climate (BWh) according to the Koppen-Geiger climate classification (Abulibdeh, 2021). The winter season extends between November and March, and is characterized by low humidity and warm temperatures, while the summer is scorching. The mean annual temperature in the Al-Batinah area ranges from 32 ℃ to 38 ℃, and decreases in the mountains; whereas precipitation is scarce and erratic, with an average annual rainfall of approximately 100 mm (Al-Hatrushi, 2013; Al-Rahbi et al., 2019). The rainfall over mountains is an essential factor contributing to the construction of plains by spreading sediments (Abulibdeh et al., 2021). Thus, the plain contains numerous valley channels, forming a complex pattern of gravel and clay descending from the mountains and dissecting the surface to drain into the Gulf of Oman. These valley gravels reach 50 m in thickness, act as the main conduit upper catchments, and constitute the location of the major water-bearing formation. In contrast, valley fans dominate the lower parts of the Al-Batinah plain, forming a coastal plain where the surface area consists of marine and terrestrial coarse to fine sand. In general, the soil varies in the study area and can be divided into six groups: Gypsiorthids, Rock outcrop-torriorthents, Torrifluvents-Torriorthents, Torriorthents (extremely gravelly), Torriorthents (very gravelly), and Torripsamments (Fig. 1C).

3. Materials and methods

The methodological approach is summarized in the schematic flowchart in (Fig. 2). We mainly focused on using remote sensing to determine changes in soil moisture using six common water indices. We also implemented different techniques to evaluate their ability to detect soil moisture, due to the lack of field data, including (1) threshold method, (2) spectral curve performance, and (3) soil-line method.

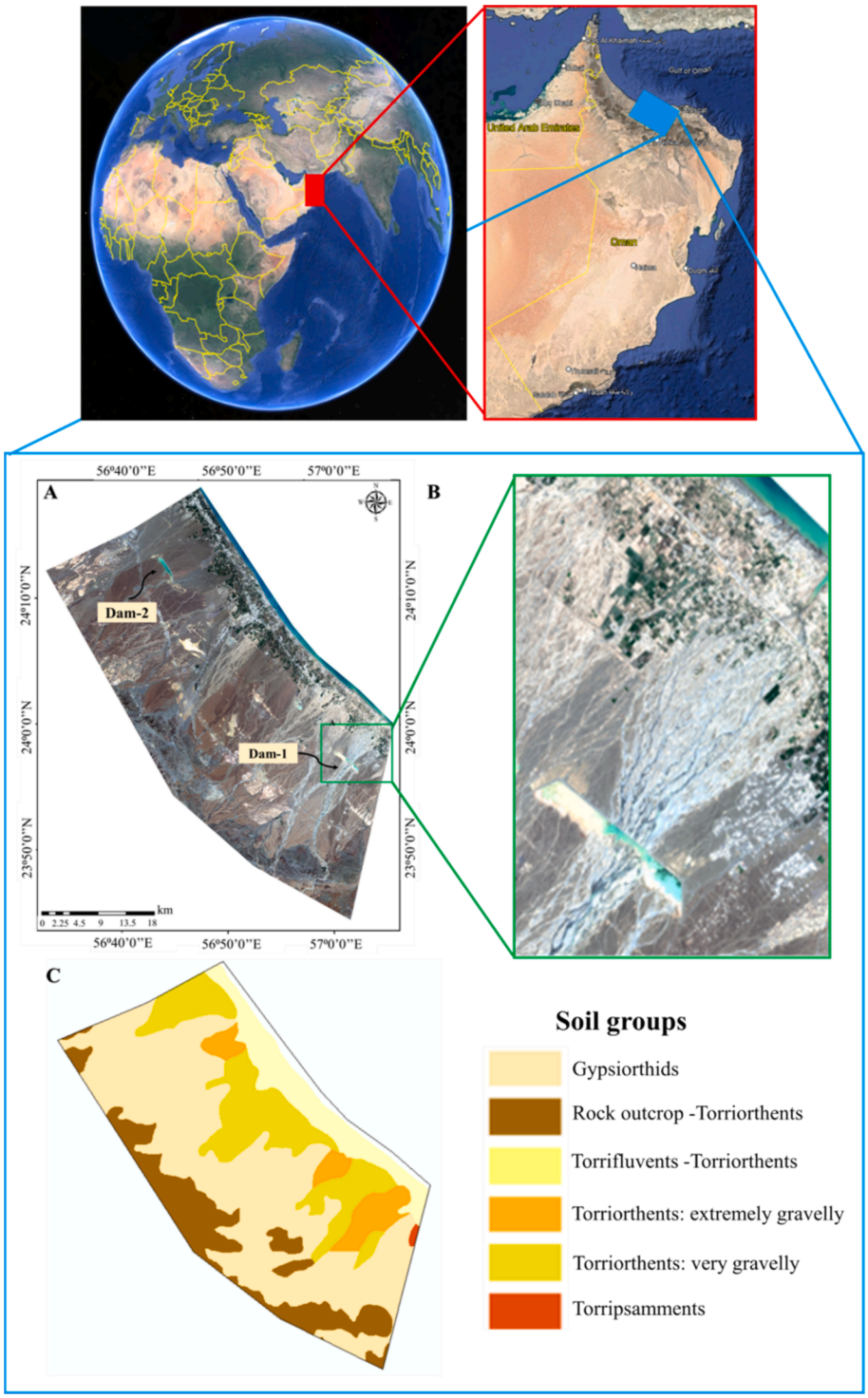

Fig. 1. (A) Study area: Sentinel 5th Oct 2021. (B) Highlighted area represents dam and narrow streams. (C) Soil map.

4. Data collection

4.1. Satellite imagery

To investigate the temporal changes in soil moisture and inundated areas, two multispectral sentinel-2 images were acquired pre-cyclone, and five were acquired post-cyclone (Table1). The time interval between two images is five days. Image-Oct^{5th} was considered a reference image because it was acquired two days after the cyclone when water was visible in the dam and narrow streams, facilitating the identification of classes (inundated areas and soil moisture) and defining the threshold values. These images were downloaded from the United States Geological Survey (USGS) website (https://earthexplorer.usgs.gov/), with a cloud cover of less than 5 %. The utilized spectral bands were resampled at a 10 m spatial resolution before being stacked together. The main characteristics of Sentinel-2 images are presented in Table 2.

4.2. Spectral indices

In this study, we investigated the potential of six remote sensing

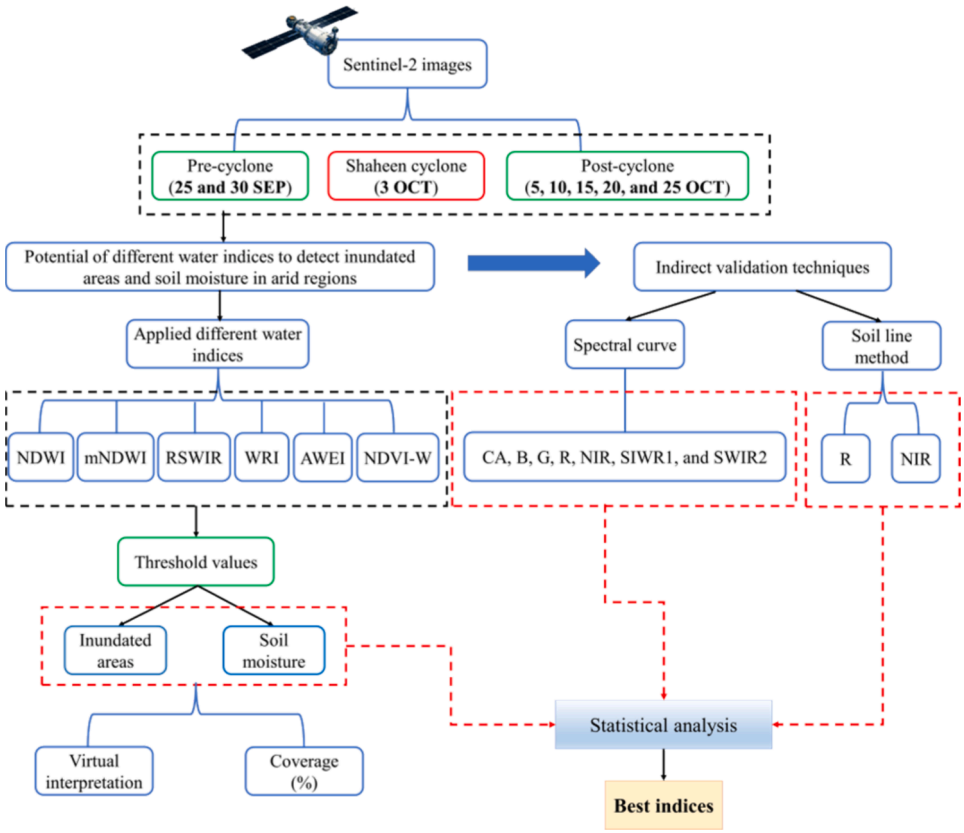

Fig. 2. A schematic flow chart represents the methodology of the current study.

Table 1
Utilized Sentinel-2 satellite imagery (pre- and post-Shaheen cyclone).

Event	Image acquisition
Pre-cyclone	25 Sep 2021
	30 Sep 2021
*Shaheen cyclone	*3 Oct 2021*
Post-cyclone	5 Oct 2021
	10 Oct 2021
	15 Oct 2021
	20 Oct 2021
	25 Oct 2021

* On Oct. 3 Shaheen cyclone hit the study area (Oman).

Table 2
Main characteristics of multispectral sentinel-2 images.

Bands Number	Bands Name	Resolution (m)	Central wavelength (nm)	Bandwidth (nm)
B1	Coastal Aerosol	60	442.7	21
B2	Blue (B)	10	492.4	66
*B3	Green (G)	10	559.8	36
*B4	Red (R)	10	664.6	31
B5	Vegetation Red Edge	20	704.1	15
B6	Vegetation Red Edge	20	740.5	15
B7	Vegetation Red Edge	20	782.8	20
*B8	Near infrared (NIR)	10	832.8	106
B8A	Vegetation Red Edge	20	864.7	21
B9	Water Vapour	60	945.1	20
B10	SWIR-Cirrus	60	1373.5	31
* B11	Short-wave Infrared (SWIR1)	20	1613.7	91
* B12	Short-wave Infrared (SWIR2)	20	2202.4	175

* The utilized spectral bands to calculate the indices. The SWIR1 and SWIR2 bands were resampled at a spatial resolution of 10 to standardize them with B, G, R, and NIR bands.

indices to extract surface water (inundated areas) and soil moisture in arid regions, as shown in Table 3. The first index is the Normalized Difference Water Index (NDWI), developed by McFeeters (1996) to detect surface water. The structure of this index is similar to that of the Normalized Difference Vegetation Index (NDVI), but relies on different spectral bands, including the green (G) and near-infrared (NIR) bands. The second index was the Modified Normalized Difference Water Index (mNDWI) developed by Xu (2006). This index replaces the NIR band with a short-wave infrared (SWIR) band to suppress the mixing of pixels of the water class with built-up lands and soil classes. The mNDWI index is considered the most common water index utilized worldwide using different satellites, including Landsat (Li et al., 2016; Acharya et al., 2018), and Sentinel (Bhangale et al., 2020). The third index is RSWIR. Rogers and Kearney (2004) replaced the G band with the R band to map surface water. This index provides good results for delineating water bodies during floods. The fourth index is the Water Ratio Index (WRI) proposed by Shen and Li (2010), which focuses on four different bands: G, R, NIR, and SWIR2. For the delineation of surface water in urban areas, Feyisa et al. (2014) proposed a fifth index called the Automated Water Extraction Index (AWEI), which is based on four bands, including B, G, NIR, SWIR1, and SWIR2. This index was intended to improve surface water extraction in areas with shadows and dark surfaces. Finally, the vegetation index (NDVI) was used to detect water and soil moisture, with values ranging from −1 to +1 (Rouse et al., 1973). The

Table 3
Utilized water indices and soil indices.

Index	Abbreviation	Formula	References
Normalized Difference Water Index	NDWI	G-NIR/G + NIR	(McFeeters, 1996)
Modified Normalized Difference Water Index	mNDWI	G-SWIR1/G + SWIR1	(Xu, 2006)
RSWIR	RSWIR	R-SWIR1/R + SWIR1	(Rogers and Kearney, 2004)
Water Ratio Index	WRI	G + R/NIR + SWIR2	(Shen and Li, 2010)
Automated Water Extraction Index	AWEI	B + 2.5*G-1.5*(NIR + SWIR1)-0.25*SWIR2	(Feyisa et al., 2014)
Normalized Difference Vegetation Index	NDVI (NDV1-W)	NIR-R/NIR + R	(Rouse Jr et al., 1973)

positive values range from 0.1 to 1, indicating sparse vegetation to dense vegetation, and zero values correspond to bare soil, while negative values indicate water. In this study, we have added the letter W to the index (NDVI-W), referring to the use of negative values to detect water in the soil.

4.3. Extract classes using thresholding method

The thresholding method was used to define and extract inundated areas (water) and soil moisture in arid regions. This method is typically used to classify and detect edges between two different classes, where each class has similar pixel values and characteristics (Balaji and Sumathi, 2014). In this study, we have extracted the threshold values of water (inundated areas) and soil moisture classes for each examined index from the Oct^{5th} (reference) and Oct^{10th} images, respectively. In the Oct^{5th} image, water pixel values were extracted from dams and streams, where they were visually identified, as shown in Fig. 1. Meanwhile, we extracted the pixel values of soil moisture from the Oct^{10th} image (after five days of reference image) in areas that obviously dried, assuming that they changed from inundated to highly moisturized areas. Then, the threshold values obtained from each index were applied to all images (pre- and post-cyclone) using the decision tree method in ENVI 5.3 software, as shown in Table 4. Finally, the derived maps were visually evaluated, focusing on the highly impacted areas, such as the main dam and prominent narrow streams (Fig. 1B).

4.4. Spectral reflectance curves and soil-line method

Different spectral reflectance techniques, including curve analysis and soil line method, were implemented to evaluate the performance of the investigated indices owing to the lack of field data. These techniques are essentially based on spectral bands (Digital Numbers). A total of 300 random points were extracted from the spectral bands (Digital Numbers) of each image (pre- and post-cyclone). These points represented different classes, including water (W), soil moisture (SM), dry soil (DS), and vegetation (V). The points of the water (W) and soil moisture (SM) classes were extracted from the overlap layers of the best indices derived from the Oct^{5th} image (post-cyclone) using the thresholding method, where the classes can be easily detected.

Furthermore, spectral reflectance curves with an average of 300 points for each spectral band, including CA, B, G, R, NIR, SWIR1, and SWIR2, were developed to assess the temporal behavior of these bands with respect to soil moisture and water classes. The soil lines were built based on the NIR and R spectral bands, considering water, soil moisture, dry soil, and vegetation classes.

Table 4
Threshold values of water and soil moisture for each utilized index based on the reference image (Oct^{5th}).

Indices	Threshold values	
	Water	Soil moisture
NDWI	> 0.0419	$\geq -0.0320 \leq 0.0419$
mNDWI	> 0.0376	$\geq -0.118 \leq 0.0376$
RSWIR	> 0.1215	$\geq -0.05 \leq 0.1215$
WRI	> 1.51	$\geq 1.01 \leq 1.51$
AWEI	> -4392.75	$\geq -5507.5 \leq$ -4392.75
NDVI-W	< -0.1002	$< -0.1002 >$ -0.0374

4.5. Hypothesis and statistical analysis

Two hypotheses were addressed in the current study to validate soil moisture detection:

(1) *Spectral reflectance curve*: Soil reflectivity decreases with increasing soil water content and vice versa but varies between bands. Water absorption bands, such as SWIR1 and SWIR2, are highly sensitive to the soil water content. In wet cases, the reflectivity of these bands should be low, indicating a high absorption. Hence, the soil classes (DS, SM, and WS) can be distinguished based on these bands. If this hypothesis is supported, the One-way ANOVA test using JMP 11 software will demonstrate a significant difference between classes (DS, SM, and WS) in the SWIR1 and SWIR2 bands.
(2) *Soil line concept (NIR-R)*: The pixels located along the soil line represent bare soil of different classes, including wet soil (WS) and dry soil (DS). The pixel values of wet and dry soil are located opposite to each other on the soil line, where WS is situated on the left side and DS on the right side. If this hypothesis is supported, on Oct^{5th}, the highest number of pixels will be located on the left side (WS) representing soil moisture and then migrate gradually to the right side (DS) during the day.

5. Results

5.1. Spatiotemporal analysis of inundated areas (water) and soil moisture

Fig. 3 shows the results of the water maps derived using the six water indices according to the selected threshold for the period from Sep^{25th} to Oct^{25th} (Table 4). The dam area was highlighted as the area with the highest impact during the cyclone, including the surface water and narrow streams. According to the visual interpretation, the sensitivity of inundated areas (water) and soil moisture varied among indices, where the inundated areas (water) are represented in dark blue and soil moisture in light blue. All indices revealed a good ability to detect changes in inundated areas (surface water), especially behind the dam (Fig. 3). However, the detection of water in narrow streams and soil moisture varied among indices.

The quantitative results showed that all indices exhibited similar behavior in inundated areas (surface water) (Fig. 4A); however, variation was observed in the soil moisture (Fig. 4B). According to the one-way ANOVA statistical analysis, the inundated areas (surface water) were significantly higher on Oct^{5th} (P-value < 0.05) for all indices, which occupied 1.4 %, 1.3 %, 1.2 %, 1.1 %, 0.93 %, and 0.81 % for mNDWI, NDWI, AWEI, RSWIR, NDVI-W, and WRI, respectively. However, the inundated areas drastically decreased by an average of 38 % after five days (Oct^{10th}) and then stabilized, with slight variations represented by the remaining water trapped by dams. The pre-cyclone dates (Sep^{25th} and Sep^{30th}) also demonstrated inundated areas (surface water) not exceeding 0.3 % for all indices, which represented water surface previously trapped by a dam-2 (Fig. 5). Moreover, the soil moisture decreased gradually after the cyclone event, but it was unexpected that the soil moisture was detected pre-cyclone (Oct^{20th} and Sep^{30th}). Furthermore, among these indices, NDWI, mNDWI, and RSWIR

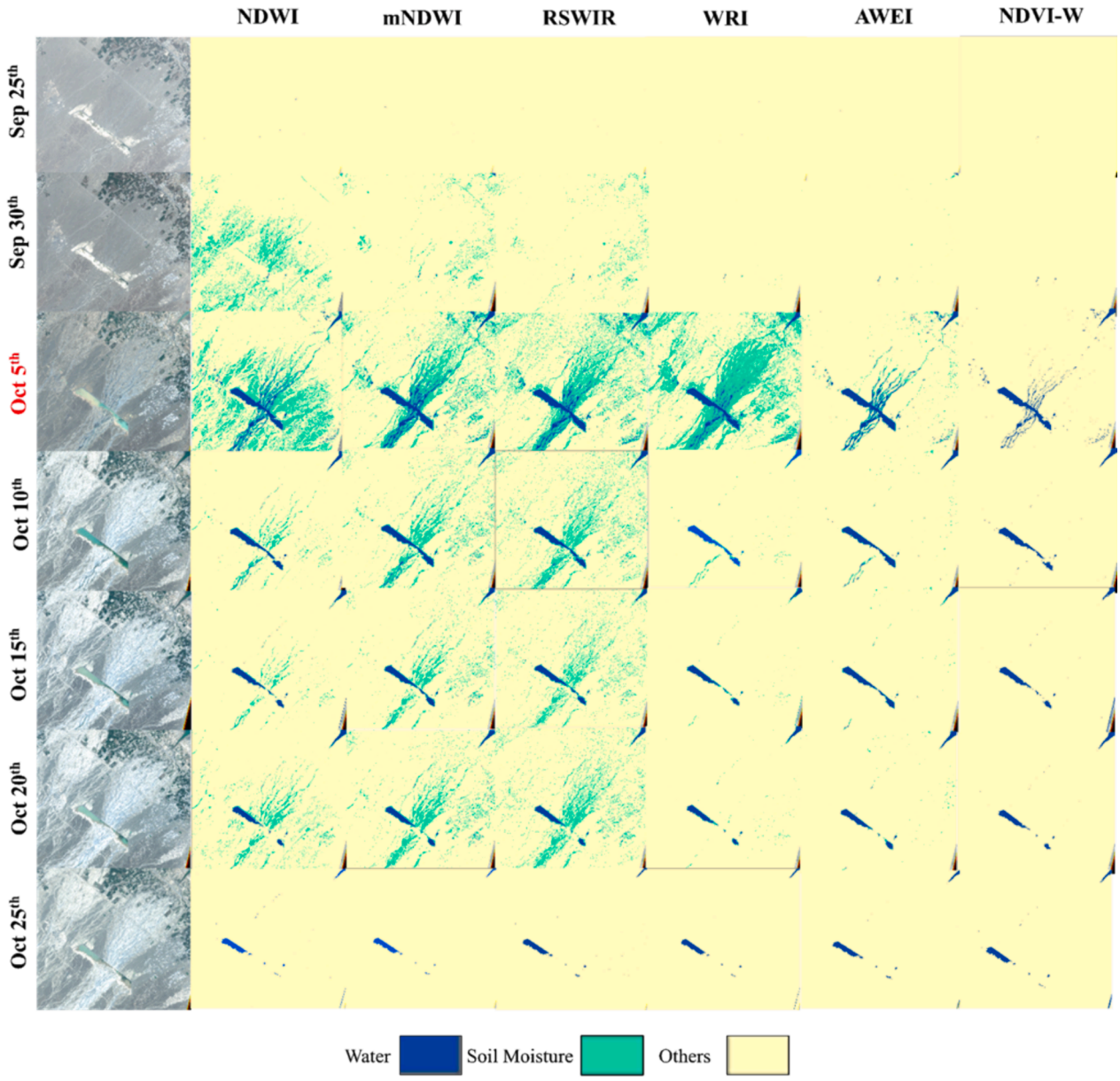

Fig. 3. True color composite images (red, green, blue) and derived water and soil moisture maps using the six considered indices, considering defined threshold values for each index (Table 4), highlighting a dam-1 area. (For interpretation of the references to color in this figure legend, the reader is referred to the web version of this article.)

exhibited similar behaviors in detecting soil moisture, with a slight overestimation observed in the NDWI index. They were also significantly higher (P-value < 0.05) on the examined dates, illustrating their ability to detect soil moisture compared to the other indices (Fig. 4B). Meanwhile, WRI and AWEI indices did not show any significant differences in soil moisture (P-value > 0.05) except on Oct^{5th}, and the NDVI-W index failed to detect the soil moisture on all examined dates (P-value > 0.05).

5.2. Assessment of temporal spectral characteristics of soil moisture and inundated areas

Our results support hypothesis 1, that soil reflectivity decreases with increasing water content, and higher absorption occurs in the SWIR1 and SWIR2 bands. Fig. 6 shows the spectral curves representing the sensitivity of each band to soil moisture and the inundated areas (water). Each curve is an average of the digital number (DN) for 300 points that were randomly selected based on the overlap of the three indices, including NDWI, mNDWI, and RSWIR. These three indices showed the best performance in discriminating between inundated areas and soil moisture, with significant differences at P-value < 0.05, as mentioned in the previous section.

The spectral band curves showed a similar trend in the soil moisture and inundated areas (water); however, the DN values varied within the curves. It was found that the reflectivity decreased with increasing soil water content and vice versa but varied between bands. The temporal DN values of soil moisture and inundated areas demonstrated low variation in the CA and visible bands (B and G), ranging between 1600 and 2000. Meanwhile, a high temporal variation in DN values was observed in the NIR, SWIR1, and SWIR2 bands in response to changes in inundated areas (water) (Fig. 6B). The DN values for the Oct^{5th} image showed a highly significant absorption of these bands (P-value < 0.05) (Fig. 7), with an average of 910 for NIR, 699 for $SWIR_1$, and 509 for $SWIR_2$, and showed differences in absorption of 60 % (NIR), 66 %

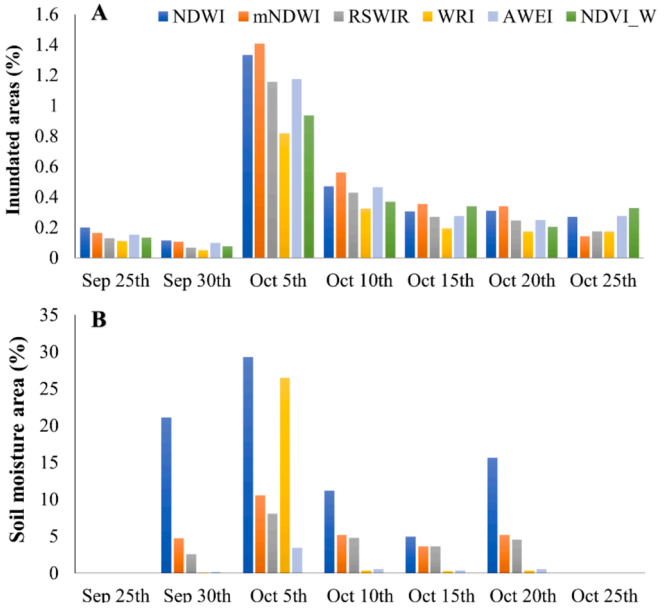

Fig. 4. Comparison of the inundated areas (A) and soil moisture (B) using different indices at different dates (Pre and Post-Cyclone).

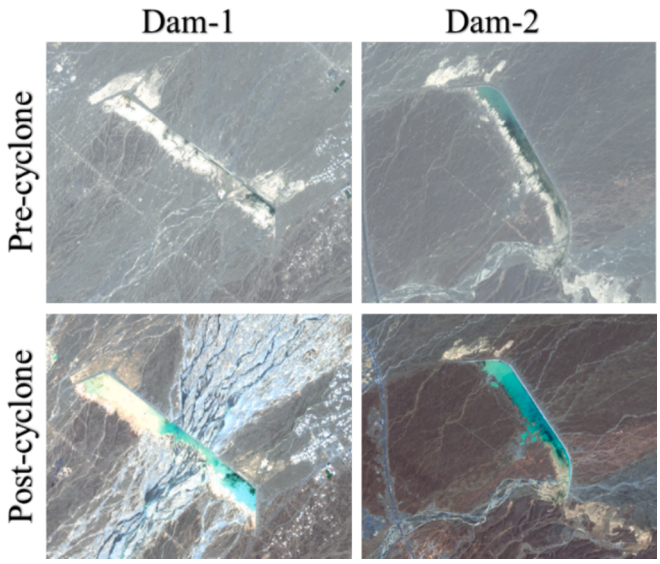

Fig. 5. Trapped water by dam-1 and dam-2 in pre-and post-cyclone.

($SWIR_1$), and 77 % ($SWIR_2$) in comparison with Sep^{30th} (Pre-Cyclone) (Fig. 6B). Subsequently, after five days (Oct^{10th}), it was found that the DN values changed in the NIR-$SWIR_{1,2}$ bands from the water (W) class to the soil wet (SW) class. The DN values for the NIR, SWIR1, and SWIR2 bands ranged from 1427 to 2005 for the NIR band, 1466–2393 for the SWIR1 band, and 1120–1913 for the SWIR2 band. However, the remaining bands, CA, B, and G, showed no significant differences between the inundated area (water) and soil moisture (SM) classes.

Furthermore, owing to the ability of the NIR, $SWIR_1$, and $SWIR_2$ bands to distinguish between the classes, a quadratic regression analysis was also performed between these significant bands and derived water index maps. The results showed that the NDWI index for all images was highly correlated with significant bands, with R^2 above 0.71 and RMSE below 0.02. However, mNDWI, RSWIR, WRI, and AWEI indices were highly correlated with $SWIR_{1,2}$ bands only on Oct^{5th}, with R^2 above 0.77 and RMSE below 0.08. An exception was observed in the NDVI index, where the result showed a weak correlation with significant bands ($R^2 \leq$ 0.35).

5.3. Assessment of soil-line behavior in considered dates

Fig. 8 shows scatterplots supporting hypothesis 2, which states that pixels migrate from wet to dry along the soil line based on water availability in the soil. According to the soil line method (red line), pixels perpendicular to the soil line (red line) upside represent vegetation. Dense and healthy vegetation (agricultural area) are represented by high digital number (DN) values in the NIR band and low values in the R band. The pixels located along the soil line represent bare soil with different classes, including wet soil (WS) and dry soil (DS). The DN values of wet and dry soils were opposite to each other on the soil line.

The results showed that the pixel distribution varied between dates (Fig. 8). On Oct^{5th} (post-cyclone), most pixels were concentrated on the left side of the soil line, representing highly wet soil. However, some pixels settled down under the soil line of wet soil (left side) because of the high absorption of R and NIR bands, representing the water class. After five days (Oct^{10th}), the distribution of pixels changed from SM to DS in response to water changes in the soil. According to spatiotemporal changes, DN values respond to soil status (W, SM, and DS), as the threshold values of the water class approximately range from 975 to 1297 for the R band and 368–951 for NIR. Meanwhile, for the SM class, the values ranged from 1298 to 2379 for the R band and 951 to 2000 for the NIR band. The DS values ranged from 2380 to 3609 for the R band and 2001 to 4047 for the NIR band.

6. Discussion

The current study indicates that the NDWI, mNDWI, and RSWIR indices derived from multispectral sentinel-2 have the potential to detect inundated areas and soil moisture in arid regions. The formulas of the three indices similar but depend on different spectral bands. Among these indices, the mNDWI and RSWIR exhibited a similar quantity of soil moisture. Meanwhile, an overestimation was observed in soil moisture for the NDWI in comparison with mNDWI and RSWIR. Replacing the NIR band in NDWI with the SWIR band in mNDWI enhanced soil moisture detection. The SWIR band is less sensitive to turbid waters with a higher concentration of sediment than the NIR band (Huang et al., 2018; Pereira et al., 2019). It is well known that the SWIR band is dedicated to discriminating between the moisture content of soil and vegetation. Hence, the interpretation of the similarity of the RWSIR index with mNDWI also relies on the SWIR band. However, the WRI, AWEI, and NDVI indices can only detect inundated areas, whereas they failed to detect soil moisture on the examined dates.

Furthermore, it seems that the WRI could detect only highly moisturized soil that occurred on Oct^{5th}, which was two days after the cyclone hit the area. Meanwhile, the AWEI index may have recognized the soil moisture that contained a high amount of clay as dark surfaces, which could explain why this index failed. The AWEI index was developed to enhance the water extraction accuracy and distinguish the boundary of water from shadows and dark surfaces (Feyisa et al., 2014). Thus, it showed excellent results in detecting surface water rather than soil moisture. For the NDVI index, the results were anticipated because it is well known that this index was developed to detect vegetation coverage within the range of 0 (non-vegetation) to 1 (high vegetation), and any values below zero correspond to water (Rouse et al., 1973).

The results also showed acceptable preliminary results for validation techniques, including the spectral reflectance curve and soil line method. These indirect validation techniques play a key role in saving time, effort, and cost, particularly for large-scale and inaccessible areas. Our study indicates that the spectral characteristics of water and soil moisture are distinct in the NIR, SWIR1, and SWIR2 bands. However, the rate and degree of absorption differ between these bands, illustrating different absorption coefficients (Yue et al., 2019). The significant relationship (P-value < 0.05) obtained between these bands and water

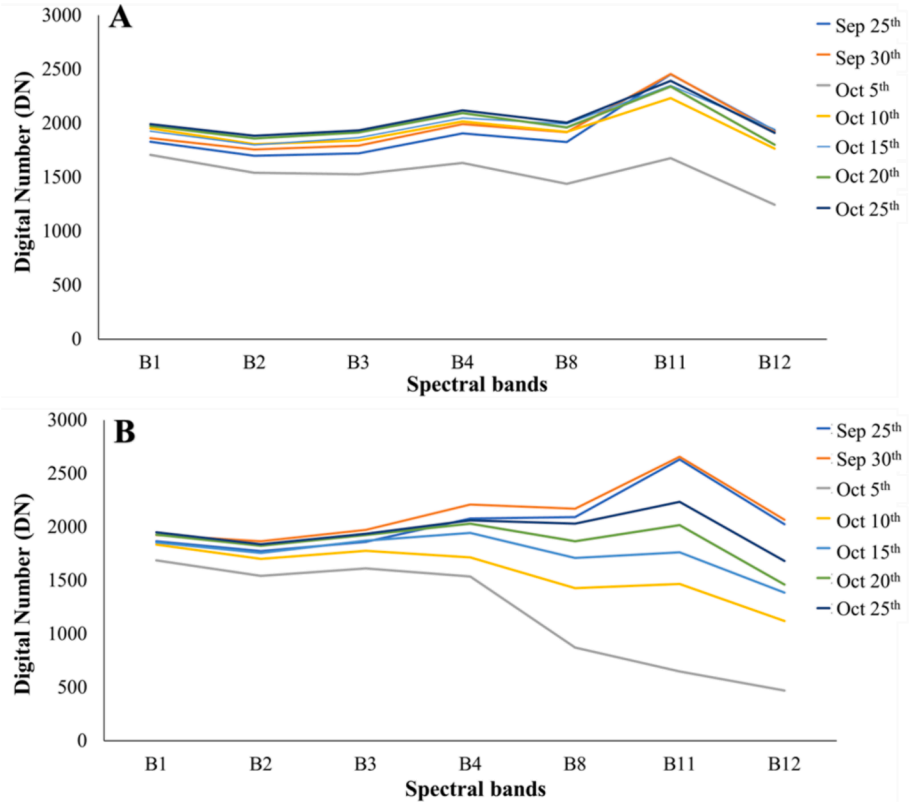

Fig. 6. Temporal spectral reflectance curve of soil moisture (A) and inundated areas (B).

indices supports an adequate selection of threshold values for these indices to detect water and soil moisture classes. This is consistent with the fact that the NIR, SWIR1, and SWIR2 bands are major water absorption bands that are highly sensitive to changes that occur in the soil (Tian and Philpot, 2015; Ngo Thi et al., 2019; Yue et al., 2019). Hence, spectral indices based on the SWIR and NIR bands often provide higher saturated soil moisture than the other bands (Yue et al., 2019).

In addition, we found that the spectral reflectance curves changed in response to water availability in the soil, especially in significant bands. The soil reflectance curve (DN) decreases as soil moisture and water increase and vice versa. This occurs because of the increased spectral forwarding scattering as a response to replacing air with water in the soil pores (Twomey et al., 1986; Yue et al., 2019). Five days after the cyclone event (Oct^{10th}), it was found that the DN values changed in NIR-SWIR1,2 bands from the water (W) class to the wet soil (WS) class in terms of an increase in reflectivity. The quantity of inundated areas also has rapidly changed, with an average decrease of 38 %. Based on the behavior of these bands, the soil moisture class can be defined with a range from 1439 to 2063.5 for the NIR band, 1677 to 2234.5 for the SWIR1 band, and 1245 to 1681 for the SWIR2 band.

The soil line results also support the appropriate selection of the threshold values of the indices. The pixel values (DN) distributed along the soil line depended on their classes. The classes that defined water (inundated area) and highly moisturized soil were located on the left side of the soil line and shifted gradually to the right side when it dried during the examined dates. These findings agree with the results obtained from the spectral reflectance curves, where the reflectivity increases during the examined dates as a response to desiccation soil. In addition, some vegetation classes disappeared from Oct^{5th} to Oct^{15th}, illustrating that agricultural areas have been covered by water.

Furthermore, selecting threshold values is challenging, where shifting from inundated areas (water) to wet and dry soil classes is still the main obstacle in understanding the behavior of spectral reflectivity. For instance, water turbidity can cause mixing between classes (Fisher et al., 2016), in terms of increasing reflectivity as a response to the suspended sediments (Garg et al., 2020). The mixed classes could also occur between turbid water containing high clay sediment and highly moisturized soil; and between areas that have changed from low soil moisture to dry soil. Therefore, selecting the indices threshold is essential for discriminating high turbid shallow water from soil moisture. We believe the threshold values vary with location, time, and seasons, as well as between indices. Thus, adjusting the threshold values is crucial in obtaining accurate results by understanding the conditions associated with the phenomenon (Huang et al., 2018).

In addition to water turbidity, different factors such as topography, soil type, and weather conditions can influence the behavior of water and soil reflectivity (Tian and Philpot, 2015; Li et al., 2016; Yumang et al., 2016; Garg et al., 2020; Du et al., 2021). For instance, surface slope plays an essential role in water movement from one area to another (Zhang et al., 2022). Surface slope controls rainfall aggregation and surface runoff occurrence, where the water velocity increases with an increase in surface slope gradients (Huang et al., 2018). Moreover, soil type affects water retention, as infiltration rates differ between soil types. Sandy soil has a strong positive relationship with the infiltration rate, whereas it is negative for clay soil (Patle et al., 2019). Clay soils have a high water-holding capacity owing to their fine particle size (high porosity and low permeability) (Patle et al., 2019; Liu et al., 2022). Unlike sandy soil, water quickly drains through coarse particles (low porosity and high permeability). In contrast, arid regions have a high evaporation rate that significantly affects soil water content (Baalousha et al., 2022). These factors are essential for interpreting the spectral reflectivity behavior and evaluating the performance of the indices. Overall, integrating these factors with the high spatial and temporal resolution of soil moisture can enhance our understanding of the probability of mudflow occurrence in arid regions.

Our study highlighted the potential of three water indices derived from multispectral sentinel-2 imagery to detect soil moisture in arid regions. Soil moisture plays a vital role in the generation of mudflows.

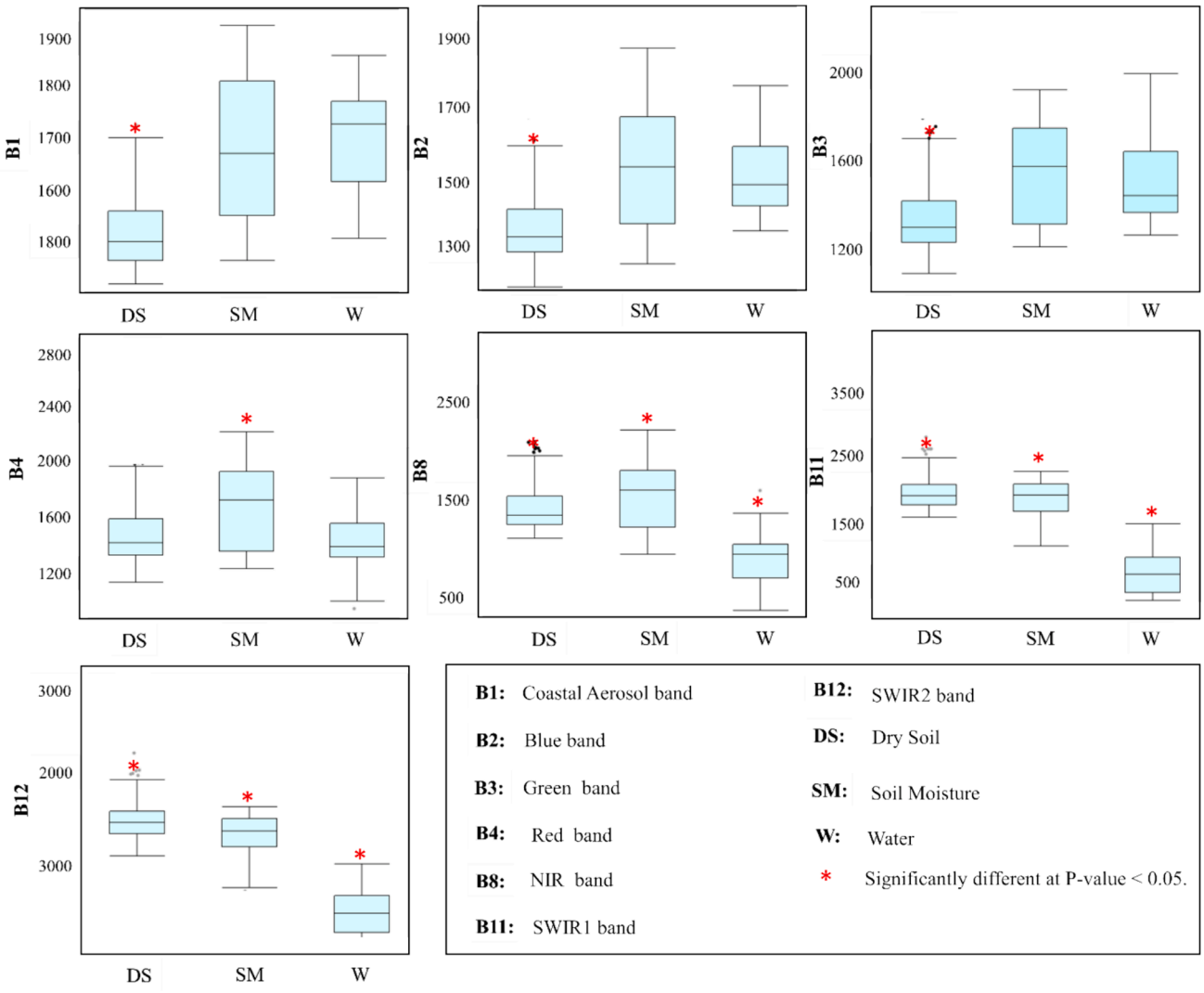

Fig. 7. Statistical relationships between bands (B1–B12) and classes (DS, SM, and W) for reference image (Oct^{5th}). *Significant difference at P-value < 0.05.

Thus, detecting soil moisture using water indices as an indicator of mudflow phenomena is crucial to predict high-risk areas and take steps to mitigate the risk. Indirect validation techniques such as spectral reflectance curves and soil line methods have been implemented in an inaccessible and large-scale area due to the impact of Shaheen cyclone. Despite obtaining acceptable preliminary results of utilized techniques. In contrast, we believe that the soil is not homogeneous, and many factors control the mudflow generation, including soil types, topography (slopes), intensity and frequency of precipitation, and vegetation coverage. Thus, adjusting threshold values in order to obtain precise predictions requires further studies that rely on field measurements. In addition, soil moisture rapidly changes and is unpredictable in arid regions due to dry climate conditions, including high temperatures, high evaporation rates, and low precipitation. Thus, the temporal resolution of free satellite imagery may not be adequate to monitor changes in soil moisture over a short time or on specific days.

Furthermore, we believe that combining field measurements with multi-sensor satellite (Landsat and Sentinel) and Unmanned Aerial Vehicles (UAVs) imageries will help in defining the threshold values, considering different aspects such as physical attributes (soil types and topography), water table fluctuations, climate conditions (low precipitation and high evaporation rate), and climate change. The combination of field measurements and remote sensing technologies will also improve long-term monitoring, where Sentinel will fill the gap in Landsat at large-scale monitoring and UAVs for small scale and during cloudy days. Our study also recommended conducting more studies using an integrating approach of using multi-spectral bands (NIR, SWIRs, and thermal bands), artificial intelligence, and spectroradiometer to enhance soil moisture prediction and develop new models that are applicable to arid regions considering different environmental aspects.

7. Conclusion

This study highlights the effectiveness of remote-sensing techniques for estimating soil moisture prediction as an indicator of mudflow in low-slop topography and areas containing clay soil. The multispectral Sentinel-2 data provided adequate spatial and temporal resolution data that permitted monitoring soil moisture changes in arid regions. As soil moisture plays a crucial role in flood and mudflow phenomena, water indices can be utilized to detect soil moisture and predict high-risk mudflow areas in arid regions. Among the examined indices, the results showed that the NDWI, mNDWI, and RSWIR indices had the potential to detect soil moisture once the threshold values for classes were adjusted correctly. The study also showed that indirect validation techniques, including spectral reflectance curve analysis and soil-line method, can help evaluate the performance of indices, especially for inaccessible and large-scale areas, in terms of saving time, effort, and

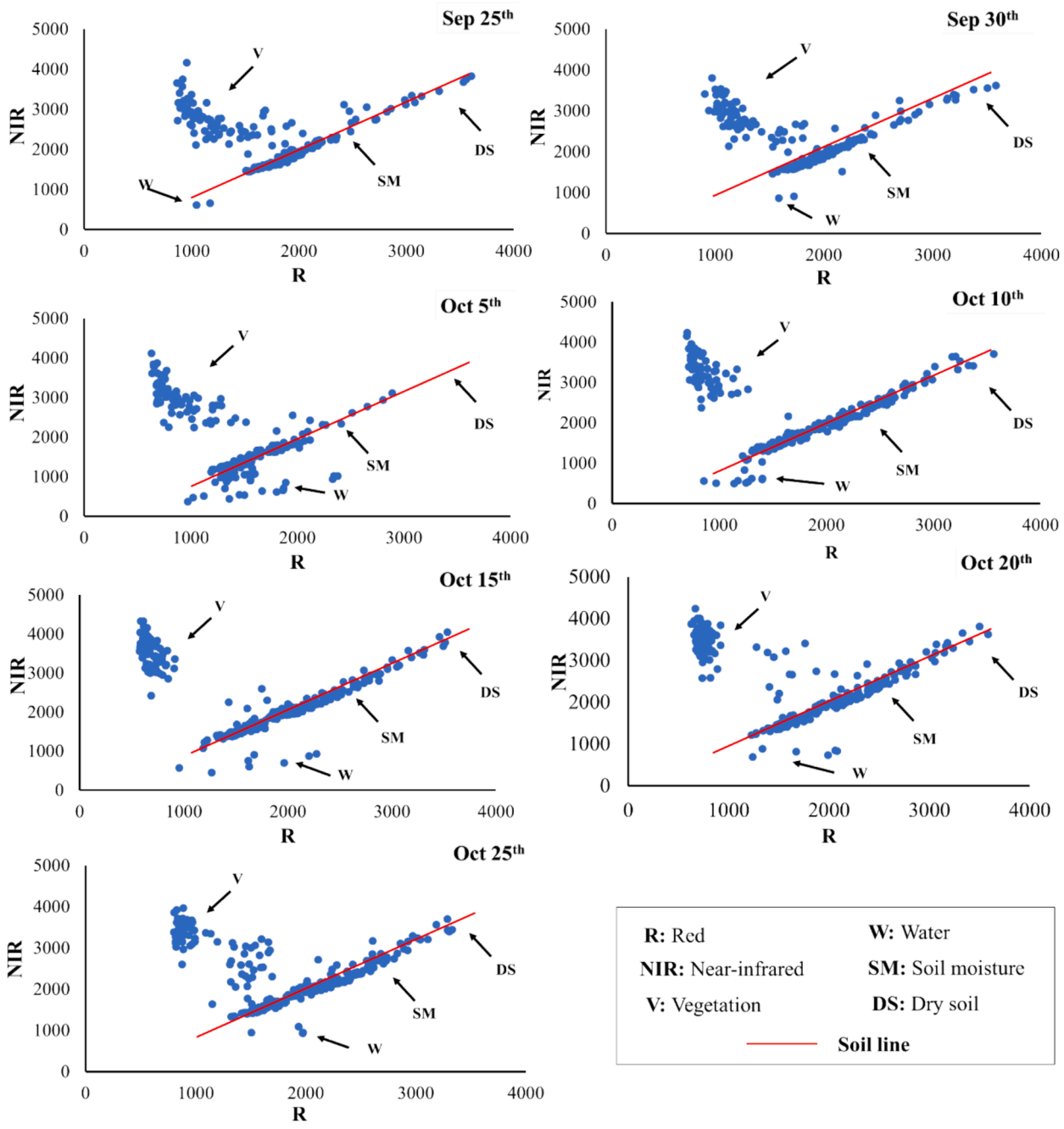

Fig. 8. Temporal distribution of pixels in R and NIR bands for inundated areas and soil moisture using Oct^{5th} image as a reference image.

cost. However, we believe that even if an index shows certain satisfactory results in a particular area, it does not mean that it will provide similar results in other areas. Therefore, testing the potential indices in different locations and validating them with fieldwork is necessary. Future studies should also be conducted to define the threshold values of soil moisture under various environmental conditions, considering seasonal variation (winter and summer) and physical attributes such as soil type and topography (low, moderate, and steep). The outcome of this study will support land-use planning projects in arid regions, particularly those affected by climate change, such as increasing the frequency and intensity of mudflow and flood events.

CRediT authorship contribution statement

Zahraa Al-Ali: . **Ammar Abulibdeh:** . **Talal Al-Awadhi:** . **Midhun Mohan:** Writing – review & editing, Methodology, Formal analysis, Conceptualization. **Noura Al Nasiri:** Writing – review & editing, Visualization, Investigation, Formal analysis. **Mohammed Al-Barwani:** Writing – review & editing, Software, Methodology, Formal analysis, Data curation. **Sara Al Nabbi:** Writing – review & editing, Visualization, Investigation, Data curation. **Meshal Abdullah:** Writing – original draft, Supervision, Methodology, Investigation, Conceptualization.

Declaration of competing interest

The authors declare that they have no known competing financial interests or personal relationships that could have appeared to influence the work reported in this paper.

Data availability

Data will be made available on request.

References

Abulibdeh, A., 2021. Analysis of urban heat island characteristics and mitigation strategies for eight arid and semi-arid gulf region cities. Environ. Earth Sci. 80 (7), 1–26.

Abulibdeh, A., Al-Awadhi, T., Al Nasiri, N., Al-Buloshi, A., Abdelghani, M., 2021. Spatiotemporal mapping of groundwater salinity in Al-Batinah, Oman. Groundwater Sust. Dev. 12, 100551.

Acharya, U., Daigh, A.L., Oduor, P.G., 2022. Soil moisture mapping with moisture-related indices, OPTRAM, and an integrated random forest-OPTRAM algorithm from landsat 8 images. Remote Sens. (Basel) 14 (15), 3801.

Acharya, T.D., Subedi, A., Lee, D.H., 2018. Evaluation of water indices for surface water extraction in a Landsat 8 scene of Nepal. Sensors 18 (8), 2580.

Al-Awadhi, T., Abdullah, M., Al-Ali, Z., Abulibdeh, A., Al-Barwani, M., Al Nasiri, N., Al-Naabi, S., Mohan, M., 2024. Navigating cyclone threats: Forecast approach using water streams' physical characteristics as an indicator to predict high risk potential areas in the Sultanate of Oman. Earth Syst. Environ. 2024, 1–13. https://doi.org/10.1007/S41748-024-00392-2.

Al-Hatrushi, S.M., 2013. Monitoring of the shoreline change using remote sensing and GIS: a case study of Al Hawasnah tidal inlet, Al Batinah coast, Sultanate of Oman. Arab. J. Geosci. 6 (5), 1479–1484.

Al-Rahbi, S.H., Al-Mulla, Y.A., Jayasuriya, H., 2019. Evaluation of salinity intrusion in arable lands of Al-Batinah coastal belt using unmanned aerial vehicle (UAV) color imagery. J. Agric. Marine Sci. [JAMS] 24, 44–50.

Baalousha, H.M., Ramasomanana, F., Fahs, M., Seers, T.D., 2022. Measuring and validating the actual evaporation and soil moisture dynamic in arid regions under unirrigated land using smart field lysimeters and numerical modeling. Water 14 (18), 2787.

Babaeian, E., Sadeghi, M., Jones, S.B., Montzka, C., Vereecken, H., Tuller, M., 2019. Ground, proximal, and satellite remote sensing of soil moisture. Rev. Geophys. 57 (2), 530–616.

Bhangale, U., More, S., Shaikh, T., Patil, S., More, N., 2020. Analysis of surface water resources using Sentinel-2 imagery. Procedia Comput. Sci. 171, 2645–2654.

Brocca, L., Crow, W.T., Ciabatta, L., Massari, C., De Rosnay, P., Enenkel, M., Hahn, S., Amarnath, G., Camici, S., Tarpanelli, A., 2017. A review of the applications of ASCAT soil moisture products. IEEE J. Sel. Top. Appl. Earth Obs. Remote Sens. 10 (5), 2285–2306.

Castro, J., Asta, M.P., Galve, J.P., Azañón, J.M., 2020. Formation of clay-rich layers at the slip surface of slope instabilities: the role of groundwater. Water 12 (9), 2639.

Cooper, J.D., 2016. Soil water measurement: a practical handbook. John Wiley & Sons.

Du, M., Zhang, J., Elmahdi, A., Wang, Z., Yang, Q., Liu, H., Liu, C., Hu, Y., Gu, N., Bao, Z., 2021. Variation characteristics and influencing factors of soil moisture content in the lime concretion black soil region in Northern Anhui. Water 13 (16), 2251.

FAO, 2021. The Impact of Disasters and Crises on Agriculture and Food Security: 2021. In: Food and Agriculture Organization of the United Nations Rome, Italy.

Feyisa, G.L., Meilby, H., Fensholt, R., Proud, S.R., 2014. Automated Water Extraction Index: a new technique for surface water mapping using Landsat imagery. Remote Sens. Environ. 140, 23–35.

Fisher, A., Flood, N., Danaher, T., 2016. Comparing Landsat water index methods for automated water classification in eastern Australia. Remote Sens. Environ. 175, 167–182.

Garg, V., Aggarwal, S.P., Chauhan, P., 2020. Changes in turbidity along Ganga River using Sentinel-2 satellite data during lockdown associated with COVID-19. Geomat. Nat. Haz. Risk 11 (1), 1175–1195.

Gheybi, F., Paridad, P., Faridani, F., Farid, A., Pizarro, A., Fiorentino, M., Manfreda, S., 2019. Soil moisture monitoring in Iran by implementing satellite data into the root-zone SMAR model. Hydrology 6 (2), 44.

Huang, C., Chen, Y., Zhang, S., Wu, J., 2018a. Detecting, extracting, and monitoring surface water from space using optical sensors: a review. Rev. Geophys. 56 (2), 333–360.

Huang, Y., Chen, X., Li, F., Zhang, J., Lei, T., Li, J., Chen, P., Wang, X., 2018b. Velocity of water flow along saturated loess slopes under erosion effects. J. Hydrol. 561, 304–311.

Ismail, S.M., Ozawa, K., 2007. Improvement of crop yield, soil moisture distribution and water use efficiency in sandy soils by clay application. Appl. Clay Sci. 37 (1–2), 81–89.

Li, Y., Gong, X., Guo, Z., Xu, K., Hu, D., Zhou, H., 2016. An index and approach for water extraction using Landsat–OLI data. Int. J. Remote Sens. 37 (16), 3611–3635.

Liu, Y., Guo, Y., Long, L., Lei, S., 2022. Soil water behavior of sandy soils under semiarid conditions in the Shendong Mining Area (China). Water 14 (14), 2159.

Lu, F., Sun, Y., Hou, F., 2020. Using UAV visible images to estimate the soil moisture of steppe. Water 12 (9), 2334.

Ma, C., Li, X., Wei, L., Wang, W., 2017. Multi-scale validation of SMAP soil moisture products over cold and arid regions in northwestern China using distributed ground observation data. Remote Sens. (Basel) 9 (4), 327.

Mamadjanova, G., Leckebusch, G.C., 2022. Assessment of mudflow risk in Uzbekistan using CMIP5 models. Weather Clim. Extremes 35, 100403.

Marino, P., Peres, D.J., Cancelliere, A., Greco, R., Bogaard, T.A., 2020. Soil moisture information can improve shallow landslide forecasting using the hydrometeorological threshold approach. Landslides 17 (9), 2041–2054.

McFeeters, S.K., 1996. The use of the Normalized Difference Water Index (NDWI) in the delineation of open water features. Int. J. Remote Sens. 17 (7), 1425–1432.

Morris, M., Energy, N., 2006. Soil moisture monitoring: low-cost tools and methods. National Center for Appropriate Technology (NCAT) 1–12.

Natsagdorj, E., Renchin, T., De Maeyer, P., Tseveen, B., Dari, C., Dashdondog, E., 2019. Soil moisture analysis using multispectral data in north central part of mongolia. ISPRS Annals of Photogrammetry, Remote Sensing & Spatial Information Sciences, 4.

Ngo Thi, D., Ha, N.T.T., Tran Dang, Q., Koike, K., Mai Trong, N., 2019. Effective band ratio of landsat 8 images based on VNIR-SWIR reflectance spectra of topsoils for soil moisture mapping in a tropical region. Remote Sens. (Basel) 11 (6), 716.

Parida, B.R., Pandey, A.C., Kumar, R., Kumar, S., 2022. Surface soil moisture retrieval using sentinel-1 SAR data for crop planning in Kosi River Basin of North Bihar. Agronomy 12 (5), 1045.

Patle, G.T., Sikar, T.T., Rawat, K.S., Singh, S.K., 2019. Estimation of infiltration rate from soil properties using regression model for cultivated land. Geol. Ecol. Landscapes 3 (1), 1–13.

Peranić, J., Čeh, N., Arbanas, Ž., 2022. The use of soil moisture and pore-water pressure sensors for the interpretation of landslide behavior in small-scale physical models. Sensors 22 (19), 7337.

Pereira, F.J.S., Costa, C.A.G., Foerster, S., Brosinsky, A., de Araújo, J.C., 2019. Estimation of suspended sediment concentration in an intermittent river using multi-temporal high-resolution satellite imagery. Int. J. Appl. Earth Obs. Geoinf. 79, 153–161.

Perera, E., Jayawardana, D., Jayasinghe, P., Bandara, R., Alahakoon, N., 2018. Direct impacts of landslides on socio-economic systems: a case study from Aranayake, Sri Lanka. Geoenviron. Disasters 5 (1), 1–12.

Rao, N.N., Rao, V.B., Ramakrishna, S., Rao, B., 2019. Moisture budget of the tropical cyclones formed over the Bay of Bengal: role of soil moisture after landfall. Pure Appl. Geophys. 176 (1), 441–461.

Reis, L.G.D.M., Souza, W.D.O., Ribeiro Neto, A., Fragoso Jr, C.R., Ruiz-Armenteros, A.M., Cabral, J.J.D.S.P., Montenegro, S.M.G.L., 2021. Uncertainties involved in the use of thresholds for the detection of water bodies in multitemporal analysis from landsat-8 and sentinel-2 images. Sensors 21 (22), 7494.

Rogers, A., Kearney, M., 2004. Reducing signature variability in unmixing coastal marsh Thematic Mapper scenes using spectral indices. Int. J. Remote Sens. 25 (12), 2317–2335.

Rouse, Jr, J. W., Haas, R. H., Schell, J., Deering, D., 1973. Monitoring the vernal advancement and retrogradation (green wave effect) of natural vegetation.

Sajjad, A., Lu, J., Chen, X., Saleem, N., 2020. Rapid riverine flood mapping with different water indexes using flood instances Landsat-8 images. Proceedings of the 5th International Electronic Conference on Water Sciences.

Şekertekin, A., Marangoz, A.M., Abdikan, S., 2018. Soil moisture mapping using Sentinel-1A synthetic aperture radar data. Int. J. Environ. Geoinform. 5 (2), 178–188.

Serrano, J., Shahidian, S., Marques da Silva, J., 2019. Evaluation of normalized difference water index as a tool for monitoring pasture seasonal and inter-annual variability in a Mediterranean agro-silvo-pastoral system. Water 11 (1), 62.

Shen, L., Li, C., 2010. Water body extraction from Landsat ETM+ imagery using adaboost algorithm. 2010 18th International Conference on Geoinformatics.

Somos-Valenzuela, M.A., Oyarzún-Ulloa, J.E., Fustos-Toribio, I.J., Garrido-Urzua, N., Ningsheng, C., 2020. Hidden hazards: the conditions that potentially enabled the mudflow disaster at Villa Santa Lucía in Chilean Patagonia. Nat. Hazards Earth Syst. Sci. 20, e2019–e2419.

Tian, J., Philpot, W.D., 2015. Relationship between surface soil water content, evaporation rate, and water absorption band depths in SWIR reflectance spectra. Remote Sens. Environ. 169, 280–289.

Vallejo, L.E., 1980. Mechanics of mudflow mobilization in low-angled clay slopes. Eng. Geol. 16 (1–2), 63–70.

Volgina, L., Sergeev, S., 2021. Determination of the mean velocity of mudflows (debris flows) taking into account their life cycle. IOP Conference Series: Materials Science and Engineering.

Wang, J., Wu, F., Shang, J., Zhou, Q., Ahmad, I., Zhou, G., 2022. Saline soil moisture mapping using Sentinel-1A synthetic aperture radar data and machine learning algorithms in humid region of China's east coast. Catena 213, 106189.

Wen, Z., Zhang, C., Shao, G., Wu, S., Atkinson, P.M., 2021. Ensembles of multiple spectral water indices for improving surface water classification. Int. J. Appl. Earth Obs. Geoinf. 96, 102278.

Xu, H., 2006. Modification of normalised difference water index (NDWI) to enhance open water features in remotely sensed imagery. Int. J. Remote Sens. 27 (14), 3025–3033.

Younis, S.M.Z., Iqbal, J., 2015. Estimation of soil moisture using multispectral and FTIR techniques. Egypt. J. Remote Sens. Space Sci. 18 (2), 151–161.

Yue, J., Tian, J., Tian, Q., Xu, K., Xu, N., 2019. Development of soil moisture indices from differences in water absorption between shortwave-infrared bands. ISPRS J. Photogramm. Remote Sens. 154, 216–230.

Yumang, A.N., Paglinawan, A.C., Perez, L.A.A., Fidelino, J.F.F., Santos, J.B.C., 2016. Soil infiltration rate as a parameter for soil moisture and temperature based Irrigation System. 2016 6th IEEE International Conference on Control System, Computing and Engineering (ICCSCE).

Zhang, Y., Liang, S., Zhu, Z., Ma, H., He, T., 2022b. Soil moisture content retrieval from Landsat 8 data using ensemble learning. ISPRS J. Photogramm. Remote Sens. 185, 32–47.

Zhang, X., Zhang, T., Zhou, P., Shao, Y., Gao, S., 2017. Validation analysis of SMAP and AMSR2 soil moisture products over the United States using ground-based measurements. Remote Sens. (Basel) 9 (2), 104.

Zhang, B., Zhang, M., Liu, H., Sun, P., Feng, L., Li, T., Wang, Y., 2022a. Water flow characteristics controlled by slope morphology under different rainfall capacities and its implications for slope failure patterns. Water 14 (8), 1271.
Zhao, B., Dai, Q., Zhuo, L., Zhu, S., Shen, Q., Han, D., 2021. Assessing the potential of different satellite soil moisture products in landslide hazard assessment. Remote Sens. Environ. 264, 112583.
Zribi, M., Muddu, S., Bousbih, S., Al Bitar, A., Tomer, S.K., Baghdadi, N., Bandyopadhyay, S., 2019. Analysis of L-band SAR data for soil moisture estimations over agricultural areas in the tropics. Remote Sens. (Basel) 11 (9), 1122.